

Supporting Information

Characterization of Densification Behavior and Mechanical Properties of Solid Electrolyte Powders for All Solid-State Batteries

Seung-Yong Lee^{a,†}, Ji-Hoon Han^{b,c,†}, Hyun-Woo Gong^d, Jae-Pyoung Ahn^d, Kyung-Woo Yi^b

Young Whan Cho^{c}*

^aMaterials Characterization Center, Korea Institute of Materials Science (KIMS), Changwon
51508 Republic of Korea

^bDepartment of Materials Science and Engineering, Seoul National University, Seoul 08826,
Republic of Korea

^cCenter for Hydrogen Energy Materials, Korea Institute of Science and Technology (KIST),
Seoul 02792, Republic of Korea

^dAdvanced Analysis Center, Korea Institute of Science and Technology (KIST), Seoul 02792,
Republic of Korea

Corresponding Author

* Young Whan Cho; E-mail: oze@kist.re.kr

1. Experimental

1.1 Materials Preparation: Commercial $\text{Li}_6\text{PS}_5\text{Cl}$ was supplied by POSCO JK SOLID SOLUTION. Lab-made $\text{Li}_6\text{PS}_5\text{Cl}$ and $\text{Li}_6\text{PS}_5\text{Br}$ was synthesized by ball-milling and annealing. Lithium sulfide (Li_2S , Sigma Aldrich, 99.9%), phosphorus pentasulfide (P_2S_5 , Sigma Aldrich, 99%), lithium chloride (LiCl , Sigma Aldrich, 99%), lithium bromide (LiBr , Sigma Aldrich, 99%), and lithium borohydride (LiBH_4 , Acros Organics, 95%) were used as starting materials. Stoichiometric mixtures of starting materials were placed in a 80 ml silicon nitride bowl with 30 zirconia balls (10 mm in diameter) and milled at 650 rpm for 3 hours (planetary mill, Fritsch pulverisette P7 Premium). The ball milling was paused for 5 minutes every 5 min to avoid increasing the sample temperature too much. Afterwards, it was heated at 550 °C for 10 hours under Ar atmosphere. $\text{Li}_{5.55}\text{PS}_{4.55}(\text{BH}_4)_{1.45}$, $\text{Li}_{5.15}\text{PS}_{4.15}(\text{BH}_4)_{1.85}$ were synthesized using a two-step ball-milling method, as described in the reference. ¹

1.2. Powder Compression Testing: Compressibility of SE powder was evaluated by means of an in-die uniaxial compression analysis. SE powder is filled in a zirconia mold with an 8 mm diameter, and then compressive stress is applied to the powder using a stainless-steel plunger with a crosshead speed of 1 mm/min. In uniaxial die compression tests, the mold material is subjected to radial stress. The maximum stress applied in the present experiment is significantly lower than the compressive strength of the zirconia mold. The typical compressive strength of zirconia is approximately 2000 MPa, and its elastic modulus exceeds 90 GPa. ² Compression test results conducted using a stainless steel mold could reproduce nearly identical results to those obtained with the zirconia mold, confirming that the influence of mold deformation is negligible.

Under compressive stress, the relative density of a compressed pellet, ρ_{relative} , was calculated using the equation (1);

$$\rho_{\text{relative}} = \text{density of compressed pellet} / \text{theoretical density of solid electrolyte} \quad (1)$$

where the density of compressed pellet is calculated by the volume of the pellet divided by the mass of the powder filled in the mold.

In order to calculate the volume change of the pellet corresponding to the compressive stress, Digital Image Correlation (DIC) analysis was conducted to measure the height of the pellet in real-time. DIC analysis is a real-time camera-based method enabling to track local displacement and deformation in selected areas. The movement of the plunger was captured by a digital camera (2752×2200 pixels) with sufficient high-time resolution (3 fps). Next, the displacement was analyzed by the DIC software, GOM Correlate 2019. Because random patterns are required for digital image tracking in DIC analysis, the upper and lower plunger were decorated by white silica sand particles on black carbon tape to form a speckle pattern before the testing. In order to achieve a height of 5 mm for all the pellets after compression, the amount of powder to be compressed was calculated for each sample based on the theoretical density. The theoretical densities of $\text{Li}_6\text{PS}_5\text{Cl}$ and $\text{Li}_6\text{PS}_5\text{Br}$ were calculated to be 1.64 g/cm^3 and 1.90 g/cm^3 , respectively. However, the theoretical density of the BH_4 -substituted sample could not be calculated with sufficient accuracy. Therefore, we assumed the theoretical density derived from the Rietveld refinement based on the measured XRD data (approximately 1.45 g/cm^3).

1.3. Ion Milling System-Scanning Electron Microscope (IMS- SEM): In order to measure the porosity in the uniform cross-section of the SSE pellets, the sample was cross-milled. Using ion milling system (IMS, ArBlade 5000, Hitach High-Tech Inc.) equipped with an Ar ion gun, it was operated at an acceleration voltage of 6 kV, a milling angle of 40° , a swing rate of 5 rpm, and a milling time of 1 hour. In order to avoid the

atmospheric reaction of the sample, a air-tight holder (Hitach High-Tech Inc.) was used. Thereafter, it was transferred to a SEM (Regulus 8230, Hitachi High-Tech Inc.) to obtain the image with an acceleration voltage of 5 kV and a beam current of 15 μ A.

1.4. IMS- Nano-indenter: The hardness and elastic modulus in a uniform cross-section of the SSE pellet was measured by nanoindentation. The same conditions of IMS performed in the porosity measurement were used. After attaching the sample to a holder dedicated to the nano-indenter, it was placed in a nano-indenter equipment (Hysitron PI-85, Bruker) installed in a SEM (Nova Nano SEM, Thermofisher) to which an Ar-filled glove box is connected. Loading force 8 mN, loading time 4 seconds, holding time 2 seconds, and unloading time 4 seconds were applied. Hardness and elastic modulus were calculated by the Oliver-Pharr method embedded in the software (Hysitron Triboscan, Bruker) installed in the nano-indenter.^{3,4} The values of hardness and elastic modulus are the mean and standard deviation of five measurements at different locations in each sample.

2. Figures and Tables

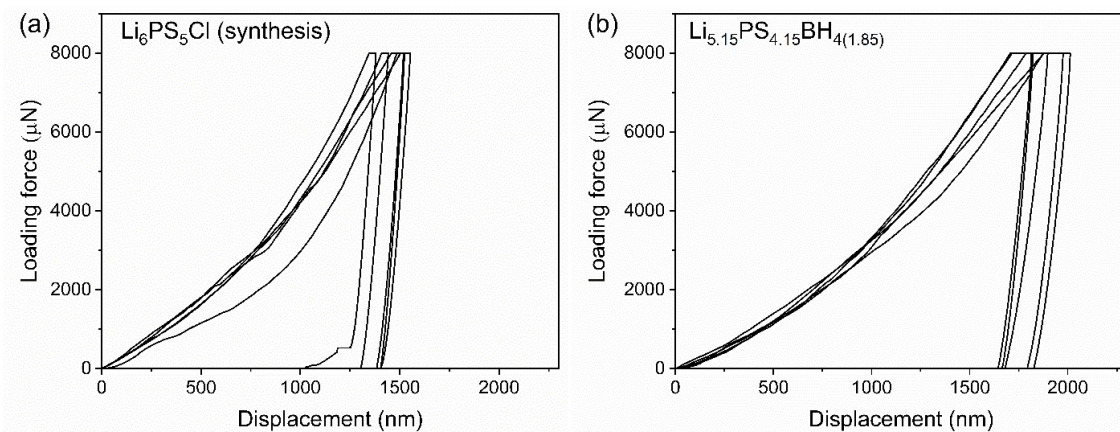


Figure S1. Indentation curve of a synthesized sample. Measurements were taken at least five times at different locations for each sample.

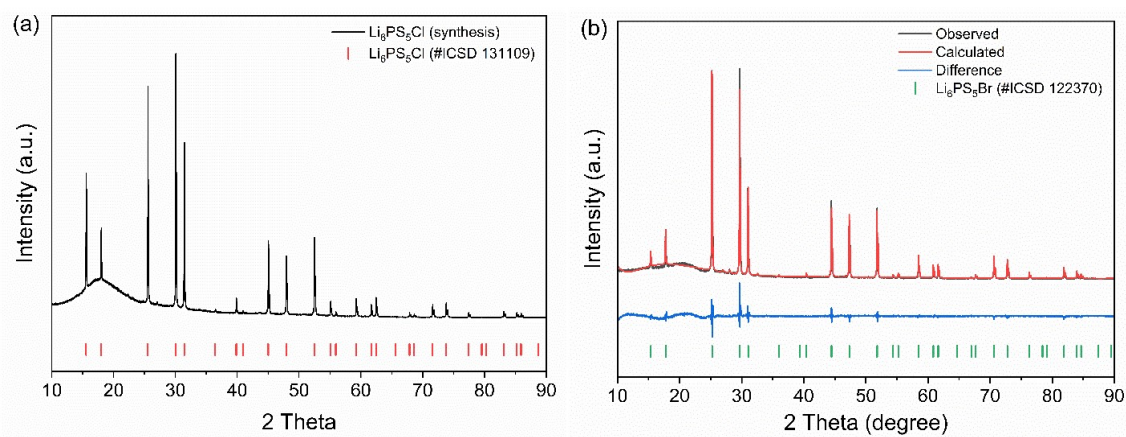
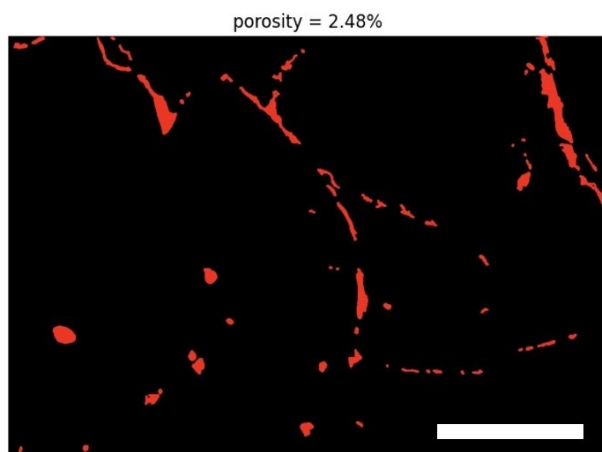
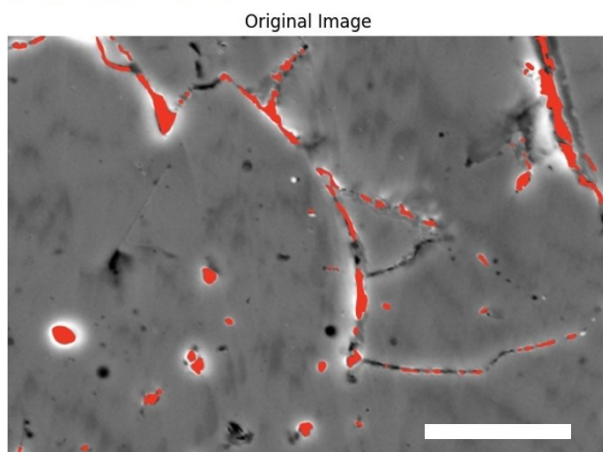
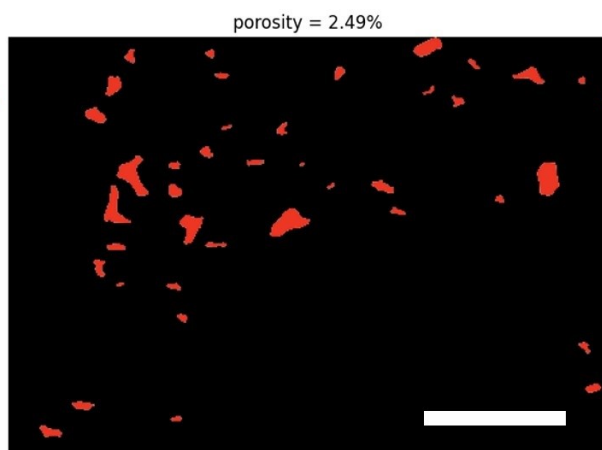
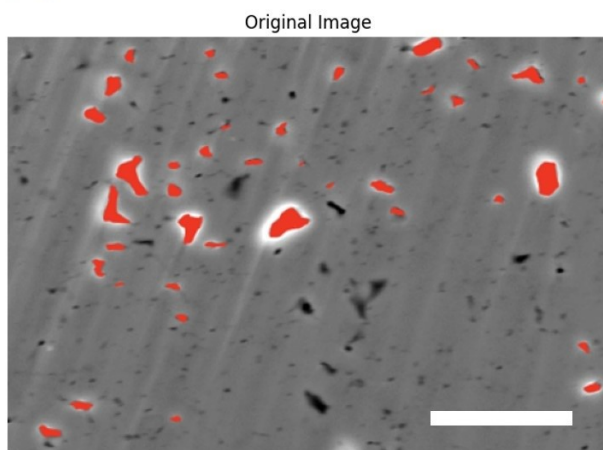


Figure S2. (a) Measured XRD data of synthesized $\text{Li}_6\text{PS}_5\text{Cl}$. (b) Rietveld refinement results of synthesized $\text{Li}_6\text{PS}_5\text{Br}$. The amorphous hump observed at angles between 10 and 20 degrees was from the Kapton film. In the case of $\text{Li}_6\text{PS}_5\text{Cl}$, only $\text{Li}_6\text{PS}_5\text{Br}$ was refined, as the distinction between S and Cl was not possible from the XRD data.

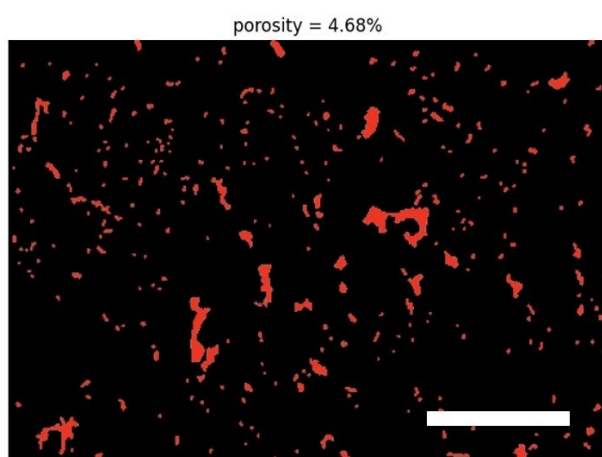
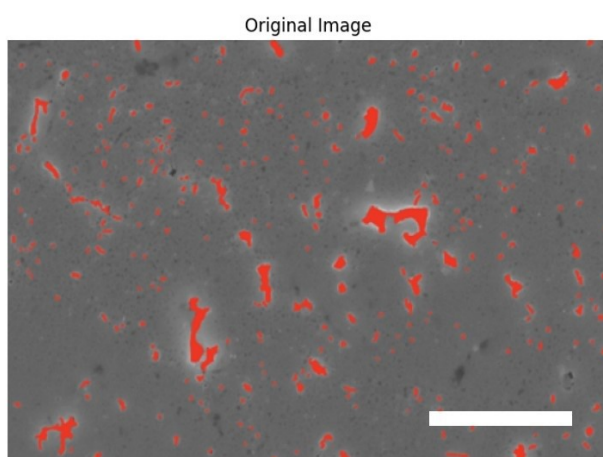
(a) $\text{Li}_6\text{PS}_5\text{Cl}$



(b) $\text{Li}_6\text{PS}_5\text{Br}$



(c) $\text{Li}_{5.55}\text{PS}_{4.55}(\text{BH}_4)_{1.45}$



(d) $\text{Li}_{5.15}\text{PS}_{4.15}(\text{BH}_4)_{1.85}$

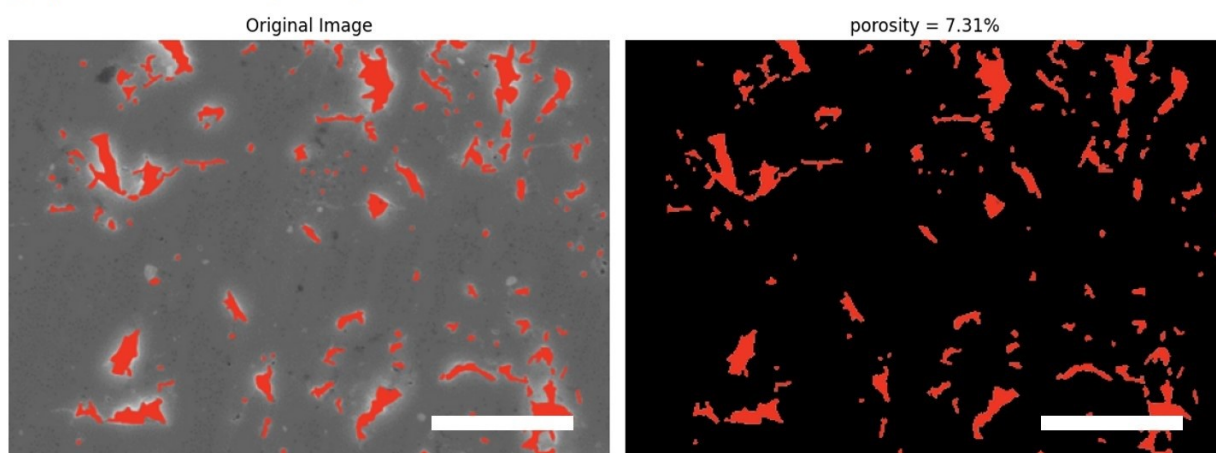


Figure S3. Cross-sectional SEM image of an synthesized electrolyte pellet (cold pressed). scale bar is $3\mu\text{m}$. The image contrast reveals black spots distributed on a gray matrix. These black spots can be categorized into two types: those with bright peripheral bands and those without. This contrast difference can be explained by the edge effect.⁵ The edge effect is a phenomenon observed in SE images where protrusions and step edges on the sample surface appear significantly brighter. This occurs because incident electrons generate substantially more secondary electrons at edges and protrusions compared to flat regions of the specimen. In the present sample, black spots representing actual material do not exhibit the edge effect at their boundaries with the matrix. On the other hand, the regions marked in red show bright contrast at their boundaries, indicating that these are pores.

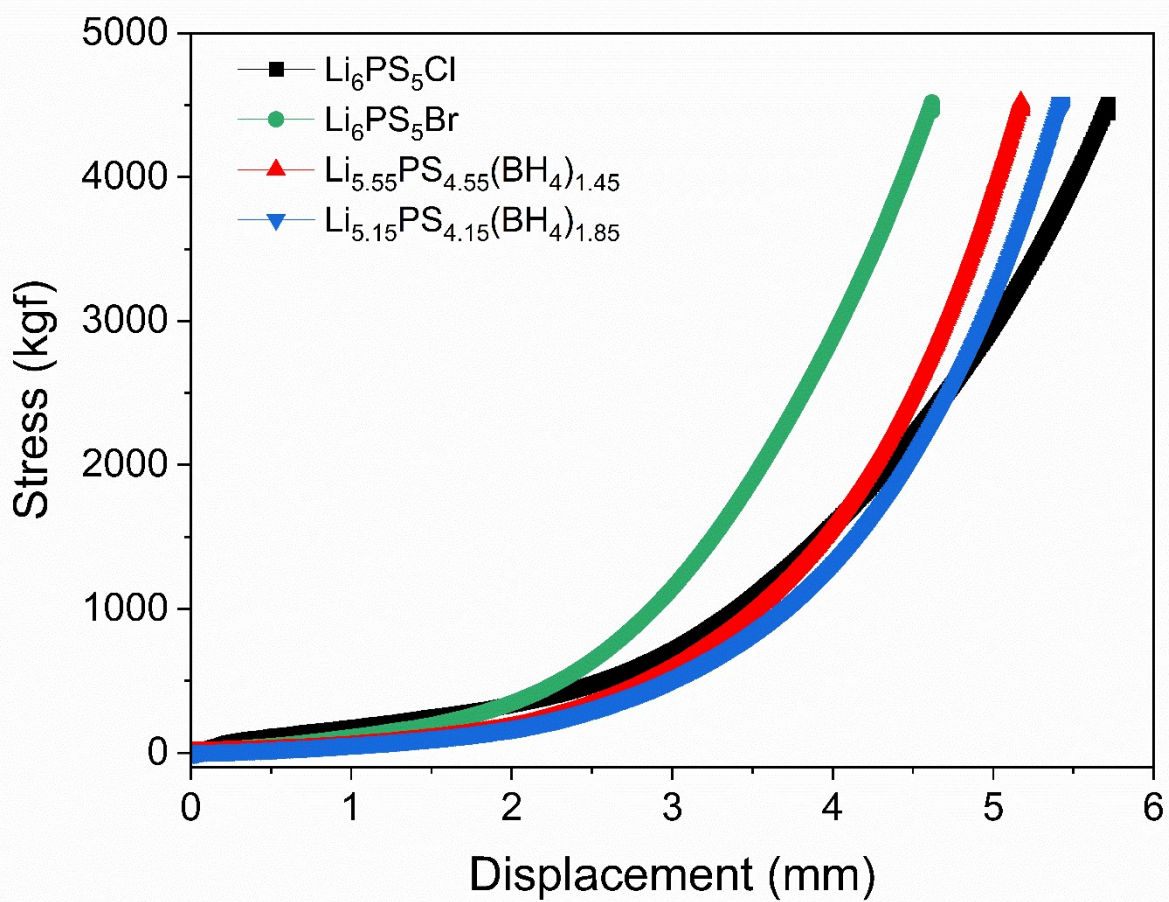


Figure S4. Raw data of powder compression test.

Table S1. Rietveld refinement results of synthesized $\text{Li}_6\text{PS}_5\text{Br}$.

(The atomic positions were taken from ICSD collection code #142464⁶)

Atom	Site	x	y	z	Occupancy
Li	48h (T5)	0.30550	0.02310	0.69450	0.492(17)
P	4b	0	0	0.5	1
S	16e	0.11920	-0.11920	0.61920	1
S	4d	0.25	0.25	0.75	0.644(8)
Br	4d	0.25	0.25	0.75	0.356(8)
S	4a	0	0	1	0.332(9)
Br	4a	0	0	1	0.668(9)
Space group, F-43m; lattice parameter, a = 9.97227(10) Å; Rwp = 8.81					

Quantitative analysis of the sample: $\text{Li}_6\text{PS}_5\text{Br} : \text{LiBr} : \text{Li}_2\text{S} = 97.3(3)\% : 0.85(8)\% : 1.9(3)\%$

3. References

1. J. H. Han, D. K. Kim, Y. J. Lee, Y. S. Lee, K. W. Yi and Y. W. Cho, *Mater Horiz*, 2023, DOI: 10.1039/d3mh01450a.
2. P. F. Manicone, P. Rossi Iommetti and L. Raffaelli, *J Dent*, 2007, **35**, 819-826.
3. Y. Jeoun, K. Kim, S.-Y. Kim, S.-H. Lee, S.-H. Huh, S. H. Kim, X. Huang, Y.-E. Sung, H. D. Abruña and S.-H. Yu, *ACS Energy Letters*, 2022, **7**, 2219-2227.
4. W. Yan, C. L. Pun, Z. Wu and G. P. Simon, *Composites Part B: Engineering*, 2011, **42**, 2093-2097.
5. K.-J. Lee, Y.-W. Byeon, H.-J. Lee, Y. Lee, S. Park, H.-R. Kim, H.-K. Kim, S. J. Oh and J.-P. Ahn, *Energy Storage Mater*, 2023, **57**, 326-333.
6. N. Minafra, M. A. Kraft, T. Bernges, C. Li, R. Schlem, B. J. Morgan and W. G. Zeier, *Inorg Chem*, 2020, **59**, 11009-11019.